



1 **Multiple scattering correction factor of quartz filters and the effect of filtering particles**
2 **mixed in water: implications to analyses of light-absorption in snow samples**

3
4
5

Jonas Svensson¹, Johan Ström², and Aki Virkkula¹

6 ¹Atmospheric Composition Research, Finnish Meteorological Institute, Helsinki, Finland

7 ²Department of Environmental Science and Analytical Chemistry, Stockholm University,
8 Stockholm, Sweden

9

10 *Correspondence to J. Svensson (jonas.svensson@fmi.fi)*

11

12 **Abstract**

13 The deposition of light-absorbing aerosols (LAA) onto snow initiates processes that lead to increased
14 snowmelt. Measurements of LAA, such as black carbon (BC) and mineral dust, have been observed
15 globally to darken snow. Several measurement techniques of LAA in snow collect the particulates on
16 filters for analysis. Here we investigate micro-quartz filters optical response to BC experiments where
17 the particles initially are suspended in air or in a liquid. With particle soot absorption photometers
18 (PSAP) we observed a 20% scattering enhancement for quartz filters compared to the standard PSAP
19 Pallflex filters. The multiple-scattering correction factor (C_{ref}) of the quartz filters for airborne soot
20 aerosol is estimated to ~ 3.4 . In the next stage correction factors were determined for BC particles mixed
21 in water and also for BC particles both mixed in water and further treated in an ultrasonic bath.
22 Comparison of BC collected from airborne particles with BC mixed in water filters indicated
23 approximately a factor of two higher mass absorption cross section for the liquid based filters, probably
24 due to the BC particles penetrating deeper in the filter matrix. The ultrasonic bath increased absorption
25 still further, roughly by a factor of 1.5 compared to only mixing in water. Application of the correction
26 functions to earlier published field data from the Himalaya and Finnish Lapland yielded MAC values
27 of $\sim 7 - 10 \text{ m}^2 \text{ g}^{-1}$ at $\lambda = 550 \text{ nm}$ which is in the range of published MAC of airborne BC aerosol.

28

29 **1 Introduction**

30 Soot consists of black carbon (BC) and organic carbon (OC) particles formed during the incomplete
31 combustion of carbonaceous fuels. As the most light-absorbing aerosol (LAA) by unit per mass, BC is
32 highly efficient in absorbing solar radiation, and is a vital component in Earth's radiative balance (Bond
33 et al., 2013). Once the particles are scavenged from the atmosphere, possibly far from their emission
34 source, BC can reach a snow surface and decrease the snow reflectivity (Warren and Wiscombe, 1980;
35 Flanner et al., 2007). This will lead to accelerated and increased snowmelt, observed in different snow



36 environments across the globe (see e.g. recent review by Skiles et al., 2018). Perhaps most notably is
37 High Mountain Asia and its extensive cryosphere, where large emission sources of LAA in close
38 proximity is affecting the region's snow and ice (e.g. Xu et al., 2009; Gertler et al., 2016; Zhang et al.,
39 2017).

40

41 Measurements of BC consists of a variety of methods, which is reflected in BC being operationally
42 defined. A common practice is to measure the change in transmission of a filter collecting aerosol. The
43 measured signal (i.e. optical depth of the filter) is thereafter applied with correction factors to generate
44 atmospheric concentrations of so-called equivalent black carbon (eBC) according to the nomenclature
45 (Petzold et al., 2013). The correction factors account for: 1) the loading of aerosol on the filter since the
46 detection signal decreases with increased aerosol content; 2) the multiple scattering of light that is
47 enhanced in the filter substrate; 3) and the enhancement from the deposition of other light scattering
48 aerosol. One instrument used for light absorption measurements is the Particle Soot Absorption
49 Photometer (PSAP), utilizing Pallflex filters. As an alternative for filter analysis of BC, another
50 approach is to apply the thermal-optical method (TOM), providing organic carbon (OC) and elemental
51 carbon (EC) mass. With this method, EC refers to the carbon content of carbonaceous matter (Petzold
52 et al., 2013). The technique involves a stepwise heating procedure, therefore creating a need to use
53 micro quartz fiber filters. These filters have been used in numerous studies with filtering snow and ice
54 samples, and thereafter analyzed to determine the EC and OC content of the samples (e.g. Hagler et al.,
55 2007; Forsström et al., 2009; Meinander et al., 2013; Ruppel et al., 2014; Zhang et al., 2017). In
56 Svensson et al. (2018), measurements with TOM were combined with an additional transmittance
57 measurement to further characterize the LAA present on the filter samples.

58

59 The goal of this paper is to further investigate micro quartz fiber filters optical behavior when sampling
60 BC particles. This aim is pursued through laboratory studies of BC filter deposition in an airborne phase,
61 as well as when the same BC particles are mixed in water and filtered onto the quartz filters (to simulate
62 snow sampling).

63

64 **2 Materials, instruments, and data analyses**

65 **2.1 Soot aerosol production and sampling**

66 A schematic picture of the experiment is presented in Fig. 1, and the methods used in each step are
67 outlined below. Soot aerosol were sampled onto filters in an airborne phase and as a part of liquid
68 solution. In the airborne aerosol tests, soot was blown into a cylindrical experimental chamber (0.8 m
69 height \times 0.45 m diameter) through a stainless steel tube (25 mm outer diameter) consisting of a y-shaped
70 bend of 130°, creating a size-separation of the aerosol. Essentially a virtual impactor, this set-up allowed



71 the smaller sized particles to continue with the airflow into the chamber, while the larger (and heavier)
72 particles were deposited into a waste pipe through inertial separation.

73

74 The soot used consisted of particles collected by chimney cleaners in Helsinki, Finland, and this
75 particular soot batch is from small-scale oil-based burning. The same soot has been applied in
76 experiments previously (Peltoniemi et al., 2015; Svensson et al., 2016; Svensson et al., 2018). From the
77 experimental chamber a sample inlet (copper, 6 mm outer diameter) simultaneously fed two PSAPs and
78 a portable aerosol spectrometer (Grimm 1.108). One of the PSAPs had quartz fiber filter punches
79 mounted, while the other had standard PSAP filters installed. This set-up was alternated among the
80 PSAPs in between the experimental runs during the experiment, to have both PSAPs assessed with the
81 different filters. In total, 22 different experimental rounds were made with various amounts of aerosol
82 deposited to the substrates.

83

84 In the liquid experiments, the same soot batch and procedure were used as above, but the outlet was
85 submerged into a 20 L container filled with deionized, purified Milli-Q (MQ) water. From this liquid
86 solution, different small amounts (between 10-100 mL) were mixed with additional MQ water to further
87 dilute the sample (to a typical total volume of 400 mL) to get a range of filters with different EC
88 concentrations and optical depths. The total number of liquid-generated filters was 35. Some selected
89 liquid samples (n=10) were exposed to an ultrasonic bath prior to filtration to further mix the soot
90 solutions. All of the liquid solutions were filtered onto the same quartz filters used in the airborne test,
91 applying the same filtering principles and analysis procedures as used previously (Svensson et al.,
92 2018). Punches from dried filters had their transmittance first measured using a PSAP, followed by EC
93 concentration measurements (TOM). This procedure was also applied to the quartz filters from the
94 airborne experiment.

95

96 **2.2 Instruments**

97 **2.2.1 Absorption measurements**

98 Absorption was measured with two Radiance Research 3-wavelength PSAPs (S/N 90 and S/N 100) at
99 $\lambda=467$ nm, 530 nm, and 660 nm (Virkkula et al., 2005). One of them was loaded with Pallflex E70-
100 2075W filter that is generally used with the instrument, while the other was loaded with micro quartz
101 fiber filters (Munktell, grade T293). The flows were calibrated with a Gilian Gilibrator bubble flow
102 meter and set to 0.5 LPM. Higher flow rates were not used here since the quartz filter tends to be more
103 fragile and may not withstand higher flows. The sample spot diameters of the PSAPs were measured
104 with an Eschenbach scale loupe with a 0.1 mm graduation ten times each. The average diameters (\pm
105 standard deviation) were 5.04 ± 0.10 mm and 5.05 ± 0.10 mm, giving corresponding spot areas of 19.9
106 ± 1.6 mm² and 20.0 ± 1.6 mm². The aim was to use identical face velocities, i.e. average velocity of



107 aerosol perpendicular to the filter (e.g. Müller et al., 2014) through both filter materials. The essentially
108 identical spot areas meant also that we had tuned the flow rates identical. In addition, to study whether
109 the PSAPs themselves affect the results we used both filter materials alternatingly, as mentioned above,
110 resulting in half of the 22 quartz filter samples being collected on the PSAP S/N 100, and the other half
111 on the PSAP S/N 90. Another custom-built 1-wavelength PSAP ($\lambda=526$ nm; Krecl et al., 2007) used in
112 Svensson et al (2018), was also utilized in for transmittance analysis of all the filters after their
113 production in the airborne- and liquid experiments.

114 2.2.2 EC measurements

115 Punches (typically with an area of 0.64 cm²) taken from the quartz filters were determined for their OC
116 and EC content with a Sunset Laboratory OCEC-analyzer (Birch and Cary, 1996), using the
117 EUSAAR_2 protocol (Cavalli et al., 2010). The analysis procedure is based on step-wise increases in
118 temperature in a helium atmosphere for the first stage, during which OC is detected with a flame
119 ionization detector. The second phase of the analysis consists of introducing oxygen into the
120 temperature increases and the detection of EC. Pyrolysis of OC during the first phase is monitored by a
121 continuous laser transmittance measurement. Once the transmittance has reached the initial value for
122 the filter in the second phase, a separation split-point between OC and EC is established.

123

124 2.2.3 Size distribution measurements

125 During the airborne experiments a Grimm optical particle counter (OPC, 1.108) was used as a portable
126 aerosol spectrometer for particle size distributions. The OPC have been factory-calibrated with PSL
127 spheres that are white. Their scattering cross section is larger than that of BC particles which leads to
128 underestimation of particle diameter. We did not find published Grimm 1.108 calibrations with BC
129 particles in the literature, thus we approximated the effect. By using the cross sections modeled by
130 Rosenberg et al. (2012) we estimate that the diameters presented by the OPC are possibly lower by a
131 factor of 2. In Figure 2 we present both the original size distributions and those calculated by
132 multiplying the diameters by 2.

133

134 2.3 Data processing

135 2.3.1 Calculation of absorption in aerosols

136 The PSAP has been calibrated with the standard filter material Pallflex E70-2075W by Bond et al.
137 (1999; here referred to as B1999) and Virkkula et al. (2005). Ogren (2010; here O2010) presented an
138 adjustment to the Bond et al. (1999) calibration, while Virkkula (2010; here V2010) updated the
139 Virkkula et al. (2005) calibration. In all of these the absorption coefficient is calculated as

$$140 \quad \sigma_{sp} = f(T_{r_t}) \frac{A}{Q\Delta t} \ln \left(\frac{T_{r_t - \Delta t}}{T_{r_t}} \right) - s\sigma_{sp} \quad (1)$$



141 where $f(Tr_t)$ is the loading correction function that depends on the transmittance $Tr_t = I_t/I_0$ where I_t is
 142 the light intensity transmitted through the filter at time t , I_0 the light intensity transmitted through a
 143 clean filter at time $t = 0$, A the spot area, Q the flow rate, and s the fraction of the scattering coefficient
 144 σ_{sp} that gets interpreted as absorption and gets usually called the apparent absorption and should be
 145 subtracted from the uncorrected absorption or be treated as presented by Müller et al. (2014). If apparent
 146 absorption can be considered negligible, equation 1 becomes

$$147 \quad \sigma_{ap} = f(Tr_t) \frac{A}{Q\Delta t} \ln\left(\frac{Tr_{t-\Delta t}}{Tr_t}\right) \quad (2)$$

148 In the present work, this approach was adapted for two reasons: 1) σ_{sp} was not measured during the
 149 calibration experiment and 2) the aerosol used in the experiment was very dark (soot from oil-based
 150 burning), thus the apparent absorption could be considered negligible.

151

152 The loading correction function $f(Tr)$ can be further rewritten as $f(Tr) = g(Tr)/C_{ref}$ where C_{ref} is the
 153 multiple scattering correction factor and $g(Tr)$ at $Tr = 1$ a loading correction function that equals one at
 154 $Tr = 1$ and increases when the filter gets darker, i.e., when $Tr < 1$.

$$155 \quad \sigma_{ap} = \frac{1}{C_{ref}} g(Tr_t) \frac{A}{Q\Delta t} \ln\left(\frac{Tr_{t-\Delta t}}{Tr_t}\right) \quad (3)$$

156 If there is only one time step $t = \Delta t$ and before sampling $Tr = 1$ then $Tr_{t-\Delta t} = Tr_{t=0} = 1$ and

$$157 \quad \sigma_{ap} = \frac{1}{C_{ref}} g(Tr_t) \frac{A}{V_t} \ln\left(\frac{1}{Tr_t}\right) = \frac{1}{C_{ref}} g(Tr_t) \sigma_0 \quad (4)$$

158 where V_t is the air volume drawn through the filter since the start of sampling at time t . The assumption
 159 of only one time step means (4) presents the absorption coefficient since the start of sampling on the
 160 filter. According to the Bouguer-Lambert-Beer law light intensity decreases exponentially as a function
 161 of the optical depth τ

$$162 \quad \begin{aligned} I_t &= I_0 e^{-\tau} \\ \Leftrightarrow \tau &= \ln\left(\frac{I_0}{I_t}\right) = \ln\left(\frac{1}{Tr_t}\right) \end{aligned} \quad (5)$$

163 This is relevant especially in the present study since the purpose is to improve estimation of absorption
 164 in filtered snow samples. In the analysis of a snow sample there is only one "time step": I_0 is the intensity
 165 of light transmitted through a clean filter and I_t the intensity of light transmitted through a filter through
 166 which the melted snow sample has been filtered. Here the airborne data were also treated in a similar
 167 way: for each time step absorption was calculated from (4) since the start of sampling on the filter.

168



169 **2.3.2 Calculation of C_{ref} of quartz filters**

170 Comparison of the $\sigma_{ap}(\text{quartz}) (= \sigma_{ap}(Q))$ and $\sigma_{ap}(\text{Pallflex}) (= \sigma_{ap}(P))$ and keeping the published PSAP
 171 calibration functions (B1999, O2010, and V2010) as standards for $\sigma_{ap}(P)$ we derive C_{ref} for the quartz
 172 filter by the following reasoning. If the same function $g(Tr)$ is used for calculating both $\sigma_{ap}(Q)$ and
 173 $\sigma_{ap}(P)$ and especially if the same $C_{ref} = C_{ref,P}$ of the Pallflex filter is used for both filter materials the
 174 ratio of the absorption coefficients at time t is

$$175 \frac{\sigma_{ap}(Q, C_{ref,P})}{\sigma_{ap}(P, C_{ref,P})} = \frac{\frac{1}{C_{ref,P}} g(Tr_Q) \frac{A}{V_t} \tau_Q}{\sigma_{ap}(P, C_{ref,P})} \quad (6)$$

176 If this ratio $\neq 1$ and if it is assumed that this is only due to using the same C_{ref} , for both filter materials,
 177 in other words if using filter-material-dependent C_{ref} yielded equal absorption $\sigma_{ap}(Q, C_{ref,Q}) = \sigma_{ap}(P, C_{ref,P})$
 178 then

$$179 \frac{\sigma_{ap}(Q, C_{ref,P})}{\sigma_{ap}(P, C_{ref,P})} = \frac{\frac{1}{C_{ref,P}} g(Tr_Q) \frac{A}{V_t} \tau_Q}{\sigma_{ap}(P, C_{ref,P})} = \frac{\frac{C_{ref,Q}}{C_{ref,P}} \frac{1}{C_{ref,Q}} g(Tr_Q) \frac{A}{V_t} \tau_Q}{\sigma_{ap}(P, C_{ref,P})} = \frac{\frac{C_{ref,Q}}{C_{ref,P}} \sigma_{ap}(Q, C_{ref,Q})}{\sigma_{ap}(P, C_{ref,P})} = \frac{C_{ref,Q}}{C_{ref,P}}$$

$$180 \Leftrightarrow C_{ref,Q} = \frac{\sigma_{ap}(Q, C_{ref,P})}{\sigma_{ap}(P, C_{ref,P})} C_{ref,P} \quad (7)$$

181 which means $C_{ref,Q}$ is obtained simply by multiplying $C_{ref,P}$ with the observed ratio of the absorption
 182 coefficients.

183

184 The $C_{ref,P}$ values for Pallflex E70-2075W filter were calculated here from two published calibration
 185 experiments. The loading correction function of B1999 (with the O2010 adjustment) can be
 186 reformulated as

$$187 f(Tr) = \frac{1}{1.5557 \cdot Tr + 1.0227} \quad (8)$$

188 This can be further rewritten as

$$189 f(Tr) = \frac{1}{C_{ref}} g(Tr) = \frac{1}{2.5784} \frac{1}{0.6034 \cdot Tr + 0.3966} \quad (9)$$

190 where $C_{ref} = 2.5784$. Similarly, the V2010 loading correction can be rewritten as

$$191 f(Tr) = (k_0 + k_1(h_0 + h_1 \omega_0) \ln(Tr)) = k_0 \left(1 + \frac{k_1}{k_0} (h_0 + h_1 \omega_0) \ln(Tr) \right) \quad (10)$$

$$= \frac{1}{C_{ref}} g(Tr) = \frac{1}{C_{ref}} \left(1 + \frac{k_1}{k_0} (h_0 + h_1 \omega_0) \ln(Tr) \right)$$

192 where h_0 , h_1 , k_0 , and k_1 are the constants presented in Table 1 in V2010 and the single-scattering albedo
 193 $\omega_0 = \sigma_{sp} / (\sigma_{sp} + \sigma_{ap})$. For the three wavelengths (10) becomes

$$194 f_{467}(Tr_{467}) = \frac{1}{2.653} (1 - 1.698(1.16 - 0.63 \cdot \omega_0) \ln(Tr_i)) \quad (11)$$



195
$$f_{530}(Tr_{530}) = \frac{1}{2.793} (1 - 1.788(1.17 - 0.71 \cdot \omega_0) \ln(Tr_g)) \quad (12)$$

196
$$f_{660}(Tr_{660}) = \frac{1}{2.841} (1 - 1.915(1.14 - 0.72 \cdot \omega_0) \ln(Tr_r)) \quad (13)$$

197 with $C_{\text{ref},467} = 2.653$, $C_{\text{ref},530} = 2.793$, and $C_{\text{ref},660} = 2.841$.

198 When C_{ref} has been determined it is assumed that $g(\text{Tr})$ is the same for both filter materials.

199

200 2.3.3 Calculation of mass absorption coefficient (MAC)

201 If m_{EC} is the mass of EC in the filter (corresponding to the spot area) through which the air volume of
202 V_t has flown the average mass concentration of EC in aerosol in the air volume is $c_{\text{EC,aerosol}} = m_{\text{EC}}/V_t$. If
203 σ_{ap} is the absorption coefficient calculated from (4), the mass absorption coefficient (MAC) can be
204 calculated from

205
$$\text{MAC} = \frac{\sigma_{\text{ap}}}{c_{\text{EC,aerosol}}} = \frac{\frac{1}{C_{\text{ref}}} g(\text{Tr}_t) \frac{A}{V_t} \tau}{\frac{m_{\text{EC}}}{V_t}} = \frac{\frac{1}{C_{\text{ref}}} g(\text{Tr}_t) A \tau}{m_{\text{EC}}} = \frac{\frac{1}{C_{\text{ref}}} g(\text{Tr}_t) \tau}{\frac{m_{\text{EC}}}{A}} = \frac{f(\text{Tr}_t) \tau}{m_{\text{EC}}/A} \quad (14)$$

206 This applies for aerosol but also for the snow samples since the analysis of EC mass in a filter yields
207 the mass surface density m_{EC}/A in where m_{EC} is the mass of EC in the analyzed filter spot that has the
208 area A . In Svensson et al. (2018) we calculated apparent MAC values of EC in snow samples simply
209 from $\text{MAC} = \tau/(m_{\text{EC}})$ without applying additional corrections for filter loading, neither enhanced
210 absorption by the filter medium, nor light scattering particles. Assuming that only loading and filter
211 effects apply in the experiments presented here, the apparent MAC values presented were adjusted by
212 using $f(\text{Tr}, Q) = g(\text{Tr})/C_{\text{ref}}(Q)$.

213

214 3 Results and discussion

215 3.1 Airborne aerosol experiment

216 Through our 22 airborne aerosol samples, we aimed at getting a range of transmittances and EC
217 concentrations in the filters for the regression analysis. The original goal was to control the final
218 transmittances by the length of the sampling time, however, this was not always successful (as noted in
219 Table 1). Without dilution the aerosol concentration in the mixing chamber was very high with
220 attenuation coefficients σ_0 in the range of $\sim 60000 - \sim 90000 \text{ Mm}^{-1}$ (see samples 1 and 2, Table 1).
221 Therefore we added a dilution valve (V1) and a HEPA filter (Fig. 1) after the first couple of experiment
222 runs, and had variations in the sample air to clean filtered air ratio, which lead to lower σ_0 in the range
223 of $\sim 1000 - \sim 30000 \text{ Mm}^{-1}$. The system was not always stable, resulting in different measured
224 concentrations for similar sampling times.

225



226 3.1.1 Particle size distribution

227 The average size distribution measured with the Grimm 1.108 OPC shows that most particles larger
228 than 1 μm (Fig. 2a) were efficiently removed from the air stream with the pre-separator (Fig. 1). This
229 is uncertain, however, since the OPC has been calibrated with white PSL spheres (as discussed in 2.2.3).
230 Another important point is that the lower limit of the sizes the OPC measured was 300 nm, and is
231 probably even higher due to the above-mentioned calibration error. The particle number size
232 distribution, nevertheless, suggests that there were large numbers of BC particles smaller than the OPC
233 detects since the particle number concentration increases sharply with decreasing particle diameter (Fig.
234 2a).

235

236 The mass absorption and scattering coefficients, MAC and MSC, respectively, and single-scattering
237 albedo ω_0 of single BC particles at $\lambda = 530$ nm were modeled with the Mie code of Barber and Hill
238 (1990) and the complex refractive index of $1.85 - 0.71i$ and a particle density of 1.7 g cm^{-3} . Comparison
239 of single-particle ω_0 size distribution (Fig. 2b) with the particle number size distribution (Fig. 2a)
240 suggests ω_0 varied in the range of $\sim 0.3 - 0.5$. Modeling for the size distribution measured with the OPC
241 yielded $\omega_0 \approx 0.51$ and 0.54 when using the original OPC diameters and the diameters multiplied by 2,
242 respectively. These ω_0 values can be considered as upper estimates considering that a large fraction of
243 small particles were undetected. However, to take the ω_0 uncertainty into account we calculated all
244 V2010-related values by using four ω_0 values: 0.3, 0.4, 0.5, and 0.6.

245

246 3.1.2 Estimation of the multiple-scattering correction factor C_{ref} for the quartz filter

247 Optical depths (τ) for both the Pallflex and quartz filters, $\tau(\text{P})$ and $\tau(\text{Q})$, respectively, were calculated
248 from (5) at a 1-second time resolution. The $\tau(\text{Q})$ -to- $\tau(\text{P})$ ratios – here the τ ratio – got a wide range of
249 values at 1-second time resolution but most of them were > 1 : 99.6 % of $\tau(\text{Q})/\tau(\text{P}) > 1$ and the average
250 and median ratios were 1.21 and 1.16, respectively. To study how the τ ratio depends on filter loading
251 the data were classified into transmittance bins of a 0.025 width in the $\text{Tr}(\text{P})$ range of 0.3 – 1.0 and the
252 averages and medians were calculated for each bin (shown in Fig. 3). The transmittance dependence of
253 the τ ratio of individual samples was often controversial: in some samples it decreased from the
254 beginning, in some samples it increased. We do not have an explanation of this although the high
255 concentrations in the mixing chamber – see the attenuation coefficients σ_0 in Table 1 – are probably
256 largely the factor behind this observation. However, for all data the average and median τ ratio depended
257 on the filter transmittance, so that for a fresh clean filter at $\text{Tr} > 0.9$, it was higher than for heavily-
258 loaded filters at $\text{Tr} < 0.4$ (Fig. 3). In addition to the 1-second data the τ ratio at the end of each sampling
259 period are plotted as a function of transmittance of the Pallflex filter in Fig. 3. For the end values of all
260 samples there was no clear Tr dependence.



261

262 In sample runs 4, 5, 7, 16, 18, 19, and 20 the decrease of τ was relatively slow and we considered the
263 bin averages and medians calculated from them to be the most suitable to be used for determining C_{ref} .
264 Sample 17 was also long, taking more than six minutes. Despite the similar settings used for filling the
265 mixing chamber and the diluter, the τ ratio was completely different from the rest of the samples (Fig.
266 3). This outlier was therefore excluded from the analysis.

267

268 The two correction algorithms (B1999 and V2010) were next applied to both filter materials and $\sigma_{\text{ap}}(\text{Q})$
269 and $\sigma_{\text{ap}}(\text{P})$ (at $\lambda = 530 \text{ nm}$) were calculated from (4) by using the τ bin averages and median of σ_0 and
270 then the ratio of these two, $\sigma_{\text{ap}}(\text{Q})/\sigma_{\text{ap}}(\text{P})$. When the constants within the correction methods, including
271 the C_{ref} , were the same for both filter materials the ratio is close to 1.2 (Fig. 4). As mentioned previously,
272 V2010 depends also on ω_0 , and due to the fact that we are unsure of the ω_0 of the aerosol, we present
273 four lines ($\omega_0 = 0.3$, $\omega_0 = 0.4$, $\omega_0 = 0.5$, and $\omega_0 = 0.6$) in Fig. 4. The B1999 correction yields a slightly
274 decreasing $\sigma_{\text{ap}}(\text{Q})/\sigma_{\text{ap}}(\text{P})$, suggesting that only adjusting C_{ref} would not be enough. The V2010
275 correction does not yield a clear τ dependence of $\sigma_{\text{ap}}(\text{Q})/\sigma_{\text{ap}}(\text{P})$ although it has high $\sigma_{\text{ap}}(\text{Q})/\sigma_{\text{ap}}(\text{P})$
276 values in the $\tau(\text{P})$ range 0.6 – 0.85. They correspond to the local maxima of the average and median τ
277 ratio shown in Fig. 3. Nevertheless, there is not enough data in this study to robustly test the correction
278 algorithms. Therefore, all values are calculated with both of them. We calculated next the multiple-
279 scattering correction factor C_{ref} from (7) by using the $\tau(\text{P})$ bin averages of $\sigma_{\text{ap}}(\text{Q})/\sigma_{\text{ap}}(\text{P})$. The averages
280 and standard deviations over the $\tau(\text{P},530)$ range of 1 – 0.3 and for averaging of all the four single
281 scattering albedos $\omega_0 = 0.3$, $\omega_0 = 0.4$, $\omega_0 = 0.5$ and $\omega_0 = 0.6$ are presented in Table 2. It is worth noting
282 that $C_{\text{ref}} \approx 3.4$ at $\lambda = 530 \text{ nm}$ is close with published values for another commonly used absorption
283 photometer, the Aethalometer, that uses quartz filters backed with supporting cellulose fibers. For
284 instance, values around 3.5 were reported by Segura et al. (2014), Zanatta et al. (2016), and Backman
285 et al. 2017.

286

287 3.2 Comparison of τ vs EC of soot mixed in water with airborne particles

288 The slopes of the optical depths ($f\tau$) vs. EC concentrations, when applying the transmittance-dependent
289 loading correction $f(\text{Tr}, \text{Q}, \text{V2010}, \omega_0 = 0.4)$, were different, and depended on how the soot aerosol were
290 deposited onto the filter (Fig. 6a and b). For the airborne aerosol, the slope is $6.4 \pm 0.2 \text{ m}^2 \text{ g}^{-1}$; while the
291 particles mixed in water (without the ultrasonic treatment) have a slope that is doubled ($12.6 \pm 0.5 \text{ m}^2$
292 g^{-1}). Applying $\omega_0 = 0.5$ and $\omega_0 = 0.6$ loading corrections, the slopes of the airborne particles are $6.1 \pm$
293 $0.2 \text{ m}^2 \text{ g}^{-1}$ and $5.7 \pm 0.20 \text{ m}^2 \text{ g}^{-1}$, respectively; while the slopes of the particles mixed in water (without
294 the ultrasonic treatment) are $12.0 \pm 0.4 \text{ m}^2 \text{ g}^{-1}$, and $11.3 \pm 0.4 \text{ m}^2 \text{ g}^{-1}$. The ratios for airborne to liquid
295 particles are 0.506 ± 0.026 , 0.507 ± 0.026 , and 0.508 ± 0.025 for the three choices of ω_0 in the



296 calculation. The difference in slope between the airborne and liquid particles is likely an effect of
297 penetration depth of the soot particles into the filter media, with the higher slope for liquid particles
298 reflecting a deeper penetration. Nevertheless, the ratio is named as the water-mixing factor $f_w \approx 0.51 \pm$
299 0.03 . In comparison, using $f(\text{Tr}, \text{B1999})$ for the airborne and the water-mixed particles the slopes for
300 optical depth $f\tau$ vs. EC concentration are $4.33 \pm 0.13 \text{ m}^2 \text{ g}^{-1}$ and $8.31 \pm 0.22 \text{ m}^2 \text{ g}^{-1}$, respectively,
301 providing a ratio of $f_w \approx 0.52 \pm 0.02$, essentially identical to that obtained from the V2010 correction.

302

303 The slope of $f\tau$ vs. EC of the 24 analyzed samples treated in the ultrasonic bath was even higher (Fig.
304 6a and b), reflecting a probable greater penetration depth of the particles. When $f(\text{Tr}, \text{Q}, \text{V2010})$ is
305 calculated with $\omega_o=0.4$, $\omega_o=0.5$ and $\omega_o=0.6$, the slopes of $f\tau$ vs. EC of the particles mixed in water with
306 the ultrasonic treatment were $18.7 \pm 0.8 \text{ m}^2 \text{ g}^{-1}$, $17.8 \pm 0.8 \text{ m}^2 \text{ g}^{-1}$, and $16.9 \pm 0.7 \text{ m}^2 \text{ g}^{-1}$, respectively.
307 The average \pm uncertainty of the ratios of the slopes of airborne and water-mixed particles with the
308 ultrasonic treatment is very stable, 0.34 ± 0.02 . If we consider this value to be a product of a factor f_s
309 representing the ultrasonic treatment and the above-presented factor f_w we obtain the value $f_s \approx 0.67 \pm$
310 0.04 . When $f(\text{Tr}, \text{B1999})$ is used also for the water-mixed and ultrasonic-bath-treated particles the slope
311 of corrected optical depth $f\tau$ vs. EC concentration is $12.9 \pm 0.4 \text{ m}^2 \text{ g}^{-1}$, with the corresponding $f_s \approx 0.65$
312 ± 0.03 .

313

314 The factors are used for multiplying $f(\text{Tr}, \text{Q}) = g(\text{Tr})/C_{\text{ref}}(\text{Q})$, and so another way it can be interpreted is
315 that they affect the multiple scattering correction

316

$$f_s f_w f(\text{Tr}) = \frac{1}{\frac{1}{f_s} \frac{1}{f_w} C_{\text{ref}}} g(\text{Tr})$$

317 In other words, $C_{\text{refSW}}(\text{Q}) = C_{\text{ref}}(\text{Q})/(f_w f_s)$ and $C_{\text{refW}}(\text{Q}) = C_{\text{ref}}(\text{Q})/f_w$ for BC particles mixed in water and
318 filtered through quartz filters with and without an ultrasonic bath, respectively. The values are presented
319 in Table 2. The uncertainties of $C_{\text{refW}}(\text{Q})$ and $C_{\text{refSW}}(\text{Q})$ were calculated with a standard error propagation
320 formula by using the standard deviations of C_{refS} in Table 2 and the above-presented uncertainties of f_w
321 and f_s .

322

323 To visualize the combined effects of the loading correction functions and the two factors f_w and f_s they
324 are plotted as a function of τ in Fig. 7. The corresponding transmittances are shown in the secondary x
325 axis. The range of optical depths of EC in snow presented by Svensson et al. (2018) are also shown in
326 the figure. It is obvious that the transmittances through those filters were much lower than $\text{Tr} = 0.3$ used
327 in the PSAP calibration in V2010 and even more lower than the $\text{Tr} = 0.6$ recommended in the World
328 Meteorological Organization and Global Atmosphere Watch (WMO/GAW, 2011) standard operating
329 procedures. However, since there is no published calibration for such low transmittances and high
330 optical depths τ the approach of extrapolating is the best that can be done. Figure 7 also shows how



331 V2010 and B1999 corrections are close to each other at low τ , but for dark filters at $\tau \approx 2$ there is a
332 factor of ~ 2 difference between them.

333

334 **3.3 Implications for field samples**

335 Previously published laboratory and ambient τ vs. EC regressions in Svensson et al. (2018), were
336 updated with the above-developed corrections. Svensson et al. (2018) presented linear regressions of
337 optical depth τ vs. EC of the same chimney soot we used in the present study, NIST soot (NIST-2975),
338 and field samples from the Himalaya (India), and Finnish Lapland. However, the optical depths
339 presented by Svensson et al. (2018) were measured with a custom-made PSAP of Stockholm University
340 at $\lambda = 526$ nm, not at $\lambda = 530$ nm with the Radiance Research PSAP used in the present study. Therefore,
341 before applying the corrections we examined whether the transmittances measured with these two
342 PSAPs agree. Transmittances of all Pallflex and quartz filters were measured with both instruments.
343 The resulting scatter plot (Fig. 8) shows that the agreement is excellent between the PSAPs, thus we
344 concluded that the corrections established in this paper could be done to the results presented by
345 Svensson et al. (2018).

346

347 We multiplied the τ of the laboratory data of Svensson et al. (2018) with $f_{sfwf}(Tr, V2010, \omega_o=0.4, Q)$
348 since an ultrasonic bath was used also in those experiments. The slopes of the chimney and NIST soot
349 decreased from ~ 40 m² g⁻¹ and ~ 35 m² g⁻¹ to 11.9 ± 0.9 m² g⁻¹ and 9.6 ± 0.6 m² g⁻¹, respectively (Fig. 9a
350 and b). In the scatter plot of the chimney soot the two data points with the highest EC concentration of
351 ~ 0.04 g m⁻² are possible outliers. When they are discarded from the regression the slope becomes $9.8 \pm$
352 0.5 m² g⁻¹, which is indicated by the red line in Fig. 9a. This is within the uncertainties and is essentially
353 the same as for the NIST soot.

354

355 These values are now in the order of published MACs, but for chimney and NIST soot still considerably
356 larger than the 6.4 ± 0.2 m² g⁻¹ obtained in the present work (section 3.2). The explanation to this
357 difference is not clear. However, the procedures of processing the chimney soot and the NIST soot were
358 not exactly identical to the one we used in the present work. Svensson et al. (2018) mixed both types of
359 soot manually in MQ water, added some ethanol in the solution and mixed samples with variable
360 amounts of MQ water before the ultrasonic mixing. In the present work instead, we blew the aerosol
361 through a virtual impactor into the MQ water, took samples of this solution and diluted the samples
362 before the mixing in the ultrasonic bath. The two major differences are the use of the size separation in
363 the present work and the use of ethanol by Svensson et al. (2018), with the explanation being due to
364 those.

365



366 For the re-evaluation of the field data presented by of Svensson et al. (2018) we multiplied the τ with
367 $f_w f(\text{Tr}, V2010, \omega_o=0.4, Q)$ since the field snow samples were melted and then filtered through the quartz
368 filters. The slopes of the field samples from the Indian Himalaya and from Finnish Lapland decreased
369 from $17.1 \pm 0.8 \text{ m}^2 \text{ g}^{-1}$ and $21.5 \pm 0.8 \text{ m}^2 \text{ g}^{-1}$ to $7.5 \pm 0.4 \text{ m}^2 \text{ g}^{-1}$ and $9.8 \pm 0.5 \text{ m}^2 \text{ g}^{-1}$, respectively (Fig
370 9c and 9d). All slopes above are in the range of published MAC of BC. For instance, Bond et al. (2013)
371 reviewed several articles and according to them the MAC of freshly-generated BC is approximately 7.5
372 $\pm 1.2 \text{ m}^2 \text{ g}^{-1}$ at $\lambda = 550 \text{ nm}$ and Quinn and Bates (2005) obtained MAC values ranging from 6 to 20 m^2
373 g^{-1} .
374

375 **4 Conclusions**

376 Through the airborne laboratory experiments conducted in this study we determined that the multiple
377 scattering effect is enhanced by about 20% with micro quartz filters compared to Pallflex filters. In
378 terms of the multiple-scattering correction factor, C_{ref} , of the quartz filters, we estimate it to be ~ 3.4 for
379 airborne sampled BC.
380

381 Mixing BC particles in water and filtering the solution essentially doubled the attenuation of light
382 compared to airborne generated filters. This is probably explained by the fact that in the liquid phase
383 and the subsequent filtering the soot particles penetrate deeper into the filter media. Deeper in the filter
384 substrate, it is more likely that the light absorption effects are enhanced, and that way accounting for
385 the measured higher optical depth. In the airborne phase the depositional process is most probably
386 different, with the particulates accumulating in the surface layer of the filter.
387

388 When samples were mixed in an ultrasonic bath before filtering through quartz filters the attenuation
389 was further enhanced. The hypothesis for explaining the effect of the ultrasonic bath is that it possibly
390 breaks the chain-like structure of BC particles, resulting in smaller BC particles that are able to move
391 to further depths in the filter matrix. This remains to be confirmed, and can possibly be done with an
392 electron microscopy. More research on the sampling of BC from melted snow and ice onto filter media
393 is much needed.
394

395 All these effects mean that the absorption data obtained from melted snow samples have high
396 uncertainties. However, application of the correction functions to earlier published field data from the
397 Himalaya and Finnish Lapland yielded MAC values of $\sim 7 - 10 \text{ m}^2 \text{ g}^{-1}$ at $\lambda = 550 \text{ nm}$ which is in the
398 range of published MAC of airborne BC aerosol. This gives indirect support for the validity of the PSAP
399 calibration also for darker filters than used as the limit in atmospheric measurements.
400



401 **Acknowledgements**

402 This work has been supported by the Academy of Finland consortium ‘Novel Assessment of Black
403 Carbon in the Eurasian Arctic: From Historical Concentrations and Sources to Future Climate Impacts’
404 (NABCEA project number 296302). J. Svensson acknowledges personal support from the Maj and Tor
405 Nessling foundation. J. Ström acknowledges support by the Swedish Research Council (VR 2017-
406 03758 ‘Black carbon particle size distributions from source to sink’.

407



408 **References**

- 409 Backman, J., Schmeisser, L., Virkkula, A., Ogren, J. A., Asmi, E., Starkweather, S., Sharma, S.,
410 Eleftheriadis, K., Uttal, T., Jefferson, A., Bergin, M., Makshtas, A., Tunved, P., and Fiebig, M.: On
411 Aethalometer measurement uncertainties and an instrument correction factor for the Arctic, *Atmos.*
412 *Meas. Tech.*, 10, 5039-5062, doi.org/10.5194/amt-10-5039-2017, 2017.
- 413
- 414 Barber, P. W. and Hill, S. C.: *Light scattering by particles: Computational methods*, World Scientific
415 Publishing, Singapore, 1990.
- 416
- 417 Birch, M. E. and Cary R. A.: Elemental carbon-based method for monitoring occupational exposures,
418 to particulate diesel exhaust, *Aerosol Sci. Tech.*, 25, 221–241, 1996.
- 419
- 420 Bond, T. C., Anderson, T. L., and Campbell, D.: Calibration and Intercomparison of Filter-Based
421 Measurements of Visible Light Absorption by Aerosols, *Aerosol Sci. Tech.*, 30, 582–600, 1999.
- 422
- 423 Bond, T. C., Doherty, S. J., Fahey, D. W., Forster, P. M., Berntsen, T., DeAngelo, B. J., Flanner, M. G.,
424 Ghan, S., Kärcher, B., Koch, D., Kinne, S., Kondo, Y., Quinn, P. K., Sarofim, M. F., Schultz, M. G.,
425 Schulz, M., Venkataraman, C., Zhang, H., Zhang, S., Bellouin, N., Guttikunda, S. K., Hopke, P. K.,
426 Jacobson, M. Z., Kaiser, J. W., Klimont, Z., Lohmann, U., Schwarz, J. P., Shindell, D., Storelvmo, T.,
427 Warren, S. G., and Zender, C. S.: Bounding the role of black carbon in the climate system: A scientific
428 assessment, *J. Geophys. Res.-Atmos.*, 188, 5380–5552, doi.org/10.1002/jgrd.50171, 2013.
- 429
- 430 Cavalli, F., Viana, M., Yttri, K. E., Genberg, J., and Putaud, J.-P.: Toward a standardised thermal-
431 optical protocol for measuring atmospheric organic and elemental carbon: the EUSAAR protocol,
432 *Atmos. Meas. Tech.*, 3, 79–89, doi.org/10.5194/amt-3-79- 2010, 2010.
- 433
- 434 Flanner, M. G., Zender, C. S., Randerson, J. T., and Rasch, P. J.: Present-day climate forcing and
435 response from black carbon in snow, *J. Geophys. Res.-Atmos.*, 112, D11202,
436 doi.org/10.1029/2006JD008003, 2007.
- 437
- 438 Forsström, S., Ström, J., Pedersen, C.A., Isaksson, E., and Gerland, S.: Elemental carbon distribution
439 in Svalbard snow, *J. Geophys. Res.-Atmos.*, 114, D19112, doi:10.1029/2008JD011480, 2009.
- 440
- 441 Hagler, G. S.W., Bergin, M. H., Smith, E. A., Dibb, J. E., Anderson, C., and Steig, E. J.: Particulate and
442 water-soluble carbon measured in recent snow at Summit, Greenland, *Geophys. Res. Lett.*, 34, L16505,
443 doi.org/10.1029/2007GL030110, 2007.



- 444 Gertler, C.G., Puppala, S.P., Panday, A., Stumm, D., Shea, J.: Black carbon and the Himalayan
445 cryosphere: a review. *Atmos. Environ.* 125, 404–417, doi.org/10.1016/j.atmosenv.2015.08.078, 2016.
446
- 447 Krecl, P., Ström, J., and Johansson, C.: Carbon content of atmospheric aerosols in a residential area
448 during the wood combustion season in Sweden, *Atmos. Environ.*, 41, 6974–6985, 2007.
449
- 450 Meinander, O., Kazadzis, S., Arola, A., Riihelä, A., Räisänen, P., Kivi, R., Kontu, A., Kouznetsov, R.,
451 Sofiev, M., Svensson, J., Suokanerva, H., Aaltonen, V., Manninen, T., Roujean, J.-L., and Hautecoeur,
452 O.: Spectral albedo of seasonal snow during intensive melt period at Sodankylä, beyond the Arctic
453 Circle, *Atmos. Chem. Phys.*, 13, 3793–3810, doi.org/10.5194/acp-13-3793-2013, 2013.
454
- 455 Müller, T., Virkkula, A., and Ogren, J. A.: Constrained two-stream algorithm for calculating aerosol
456 light absorption coefficient from the Particle Soot Absorption Photometer, *Atmos. Meas. Tech.*, 7,
457 4049–4070, doi.org/10.5194/amt-7-4049-2014, 2014.
458
- 459 Peltoniemi, J. I., Gritsevich, M., Hakala, T., Dagsson-Waldhauserová, P., Arnalds, Ó., Anttila, K.,
460 Hannula, H.-R., Kivekäs, N., Lihavainen, H., Meinander, O., Svensson, J., Virkkula, A., and de Leeuw,
461 G.: Soot on Snow experiment: bidirectional reflectance factor measurements of contaminated snow,
462 *Cryosphere*, 9, 2323–2337, doi.org/10.5194/tc-9-2323-2015, 2015.
463
- 464 Ogren, J. A.: Comment on calibration and intercomparison of filter-based measurements of visible light
465 absorption by aerosols, *Aerosol Sci. Tech.*, 44, 589–591, doi.org/10.1080/02786826.2010.482111,
466 2010.
467
- 468 Rosenberg, P. D., Dean, A. R., Williams, P. I., Dorsey, J. R., Minikin, A., Pickering, M. A., and Petzold,
469 A.: Particle sizing calibration with refractive index correction for light scattering optical particle
470 counters and impacts upon PCASP and CDP data collected during the Fennec campaign, *Atmos. Meas.*
471 *Tech.*, 5, 1147–1163, doi.org/10.5194/amt-5-1147-2012, 2012.
472
- 473 Ruppel, M. M., Isaksson, E., Ström, J., Beaudon, E., Svensson, J., Pedersen, C. A., and Korhola, A.:
474 Increase in elemental carbon values between 1970 and 2004 observed in a 300- year ice core from
475 Holtedahlfonna (Svalbard), *Atmos. Chem. Phys.*, 14, 11447–11460, doi.org/10.5194/acp-14-11447-
476 2014, 2014.
477
- 478 Petzold, A., Ogren, J.A., Fiebig, M., Laj, P., Li, S., Baltensperger, U., Holzer-Popp, T., Kinne, S.,
479 Pappalardo, G., Sugimoto, N., Wehrli, C., Wiedensohler, A. and Zhang, X.: Recommendations for



480 reporting black carbon measurements, *Atmos. Chem. Phys.*, 13, 8365–8379, 10.5194/acp-13-8365-
481 2013, 2013.

482

483 Quinn, P. K. and Bates, T. S.: Regional aerosol properties: comparison of boundary layer measurements
484 from ACE1, ACE2, Aerosols99, INDOEX, ACE Asia, TARFOX, and NEAQS, *J. Geophys. Res.*, 110,
485 D14202, doi:10.1029/2004JD004755, 2005.

486

487 Segura, S., Estellés, V., Titos, G., Lyamani, H., Utrillas, M.P., Zotter, P., Prévôt, A.S.H., Močnik, G.,
488 Alados-Arboledas, L., and Martínez-Lozano, J.A.: Determination and analysis of in situ spectral aerosol
489 optical properties by a multi-instrumental approach. *Atmos. Meas. Tech.* 7, 2373–2387,
490 doi.org/10.5194/amt-7-2373-2014, 2014.

491

492 Skiles, S. M., Flanner, M., Cook, J. M., Dumont, M., and Painter, T. H.: Radiative forcing by light-
493 absorbing particles in snow, *Nat. Clim. Change*, 8, 964–971, doi.org/10.1038/s41558-018-0296-5,
494 2018.

495

496 Svensson, J., Virkkula, A., Meinander, O., Kivekäs, N., Hannula, H.-R., Järvinen, O., Peltoniemi, J. I.,
497 Gritsevich, M., Heikkilä, A., Kontu, A., Neitola, K., Brus, D., Dagsson-Waldhauserova, P., Anttila, K.,
498 Vehkamäki, M., Hienola, A., de Leeuw, G., and Lihavainen, H.: Soot-doped natural snow and its albedo
499 – results from field experiments, *Boreal Environ. Res.*, 21, 481–503, 2016.

500

501 Svensson, J., Ström, J., Kivekäs, N., Dkhar, N. B., Tayal, S., Sharma, V. P., Jutila, A., Backman, J.,
502 Virkkula, A., Ruppel, M., Hyvärinen, A., Kontu, A., Hannula, H.-R., Leppäranta, M., Hooda, R. K.,
503 Korhola, A., Asmi, E., and Lihavainen, H.: Light-absorption of dust and elemental carbon in snow in
504 the Indian Himalayas and the Finnish Arctic, *Atmos. Meas. Tech.*, 11, 1403–1416, doi.org/10.5194/amt-
505 11-1403-2018, 2018.

506

507 Virkkula, A.: Correction of the calibration of the 3-wavelength Particle Soot Absorption Photometer
508 (3λ PSAP), *Aerosol Sci. Tech.*, 44, 706–712, doi.org/10.1080/02786826.2010.482110, 2010.

509

510 Virkkula, A., Ahlquist, N. C., Covert, D. S., Arnott, W. P., Sheridan, P. J., Quinn, P. K., and Coffman,
511 D. J.: Modification, calibration and a field test of an instrument for measuring light absorption by
512 particles, *Aerosol Sci. Tech.*, 39, 68–83, doi.org/10.1080/027868290901963, 2005.

513

514 Warren, S. and Wiscombe, W.: A model for the spectral albedo of snow II. Snow containing
515 atmospheric aerosols, *J. Atmos. Sci.*, 37, 2734–2745, 1980.

516



- 517 WMO/GAW: WMO/GAW Standard Operating Procedures for In-situ Measurements of Aerosol Mass
518 Concentration, Light Scattering and Light Absorption, GAW Report No. 200, World Meteorological
519 Organization, Geneva, Switzerland, 2011.
520
- 521 Xu, B., Cao, J., Hansen, J., Yao, T., Joswiak, D.R., Wang, N., Wu, G., Wang, M., Zhao, H., Yang, W.,
522 Liu, X., and He, J.: Black soot and the survival of Tibetan glaciers. *Proc. Nat. Acad. Sci. USA*, 106,
523 22114–22118, doi:10.1073/pnas.0910444106, 2009.
524
- 525 Zanatta, M., Gysel, M., Bukowiecki, N., Müller, T., Weingartner, E., Areskoug, H., Fiebig, M., Yttri,
526 K.E., Mihalopoulos, N., Kouvarakis, G., Beddows, D., Harrison, R.M., Cavalli, F., Putaud, J.P.,
527 Spindler, G., Wiedensohler, A., Alastuey, A., Pandolfi, M., Sellegri, K., Swietlicki, E., Jaffrezo, J.L.,
528 Baltensperger, U., and Laj, P.: A European aerosol phenomenology-5: climatology of black carbon
529 optical properties at 9 regional background sites across Europe. *Atmos. Environ.* 145, 346–364,
530 doi.org/10.1016/j.atmosenv.2016.09.035, 2016.
531
- 532 Zhang, Y., Kang, S., Li, C., Gao, T., Cong, Z., Sprenger, M., Liu, Y., Li, X., Guo, J., Sillanpää, M.,
533 Wang, K., Chen, J., Li, Y., and Sun, S.: Characteristics of black carbon in snow from Laohugou No. 12
534 glacier on the northern Tibetan Plateau, *Sci. Total Environ.*, 607–608, 1237–1249,
535 doi.org/10.1016/j.scitotenv.2017.07.100, 2017.



536 Table 1. Main information on aerosol samples taken during the experiment. Sampling time, Tr:
 537 transmittances of Pallflex and quartz filters at $\lambda = 530$ nm at the end of each sample, σ_0 : attenuation
 538 coefficient, calculated without any loading corrections, $\tau(Q)/\tau(P)$: ratio of optical depths of quartz and
 539 Pallflex filters and EC: EC concentration in the quartz filter. The 1-second data from samples denoted
 540 with * were used for deriving C_{ref} of quartz filters. Samples 1 and 2 were taken from the mixing chamber
 541 without any dilution.

Sample number	Sampling time min	Tr		$\sigma_0(P)$	$\sigma_0(Q)$	$\tau(Q)/\tau(P)$	EC g m ⁻²
		Tr(P)	Tr(Q)	Mm ⁻¹	Mm ⁻¹		
1	0.55	0.314	0.279	84245	92840	1.102	0.172
2	0.43	0.493	0.458	65284	72082	1.104	0.113
3	1.82	0.544	0.487	13405	15842	1.182	0.094
4*	6.7	0.543	0.509	3646	4032	1.106	0.056
5*	11.8	0.746	0.702	993	1199	1.207	0.029
6	2.68	0.543	0.505	9103	10184	1.119	0.062
7*	12.13	0.224	0.216	4932	5052	1.024	0.195
8	0.6	0.609	0.592	33062	34950	1.057	0.027
9	0.88	0.823	0.797	8821	10275	1.165	0.014
10	0.67	0.913	0.902	5461	6188	1.133	0.016
11	1.38	0.931	0.923	2067	2317	1.121	0.027
12	0.32	0.915	0.904	11221	12749	1.136	0.012
13	0.57	0.927	0.913	5351	6425	1.201	0.009
14	0.65	0.814	0.781	12664	15211	1.201	0.011
15	2.93	0.704	0.664	4786	5584	1.167	0.032
16*	11.6	0.602	0.555	1750	2030	1.16	0.029
17	6.12	0.5	0.415	4533	5751	1.269	0.080
18*	11.92	0.401	0.354	3067	3486	1.136	0.113
19*	10.47	0.302	0.262	4576	5119	1.119	0.147
20*	6.97	0.402	0.367	5232	5755	1.1	0.113
21	3.6	0.6	0.558	5676	6482	1.142	0.055
22	2.1	0.849	0.833	3118	3480	1.116	0.017

542

543 Table 2. Multiple-scattering correction factors of quartz filters. $C_{ref}(Q)$: derived here for airborne BC
 544 particles from published Pallflex filter loading corrections V2010 and O2010. $C_{refW}(Q)$: derived here
 545 for BC particles mixed in water and filtered through quartz filters. $C_{refSW}(Q)$: derived here for BC
 546 particles mixed in water and treated in an ultrasonic bath and filtered through quartz filters.

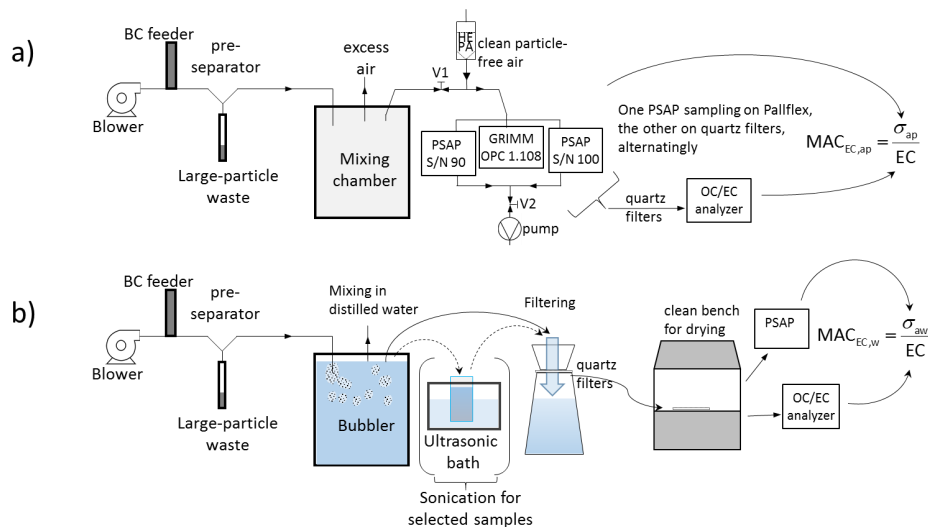
	Derived from V2010			Derived from O2010
	467 nm	530 nm	660 nm	same for all λ
$C_{ref}(Q)$	3.23 ± 0.04	3.41 ± 0.03	3.48 ± 0.09	3.08 ± 0.04
$C_{refW}(Q)$	6.4 ± 0.3	6.7 ± 0.3	6.9 ± 0.4	5.9 ± 0.2
$C_{refSW}(Q)$	9.5 ± 0.7	10.0 ± 0.8	10.2 ± 0.8	9.1 ± 0.6

547

548



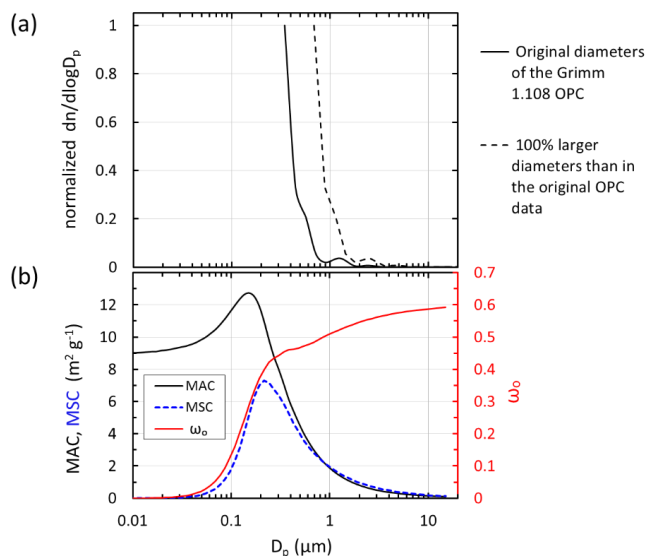
549 **Figures**



550

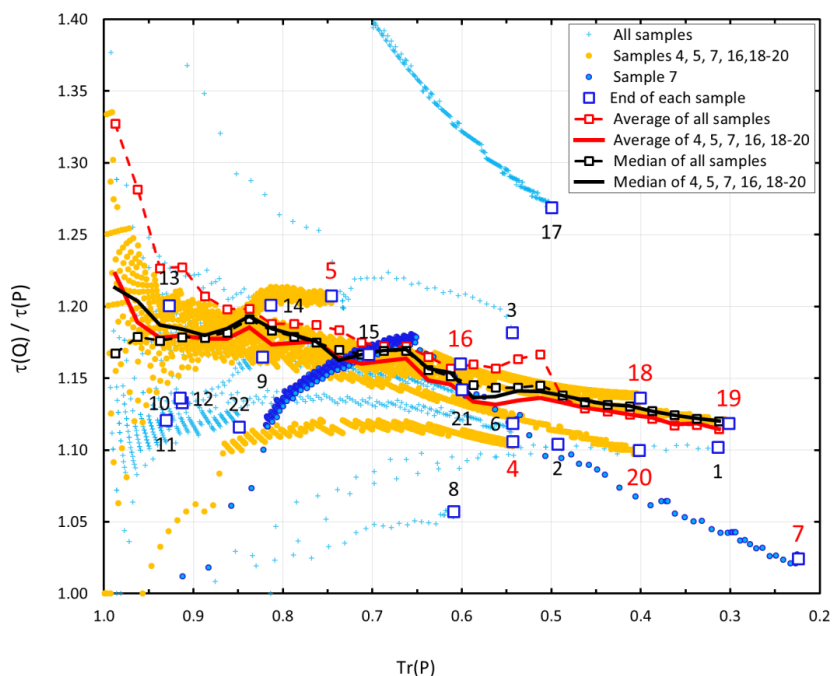
551 Figure 1. Experimental setup for the airborne (a), and for the liquid (b) procedures.

552



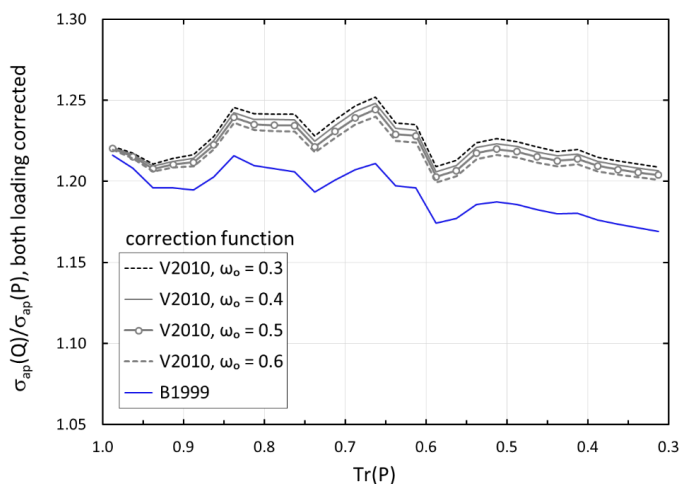
553

554 Figure 2. Size-dependent aerosol properties relevant to the experiment. a) Normalized average particle
 555 number size distribution of soot aerosol measurement in the mixing chamber with the Grimm 1.108
 556 OPC. The continuous lines present the size distributions with the original diameters of the OPC and the
 557 dashed lines those assuming that the original diameters were underestimated by a factor of 2. b) Mass
 558 absorption and scattering coefficients, MAC and MSC, respectively, and single-scattering albedo ω_0 of
 559 single BC particles at $\lambda = 530 \text{ nm}$.



560

561 Figure 3. Ratio of non-loading-corrected optical depths ($\tau = \ln(1/\text{Tr})$) of quartz and Pallflex filters, $\tau(Q)$
 562 and $\tau(P)$, respectively at $\lambda = 530$ nm at one second time resolution.. The numbers denote the value at
 563 the end of each sample. The red numbers are associated with those samples that were used for deriving
 564 $C_{\text{ref}}(\text{quartz})$ in section 3.1.2

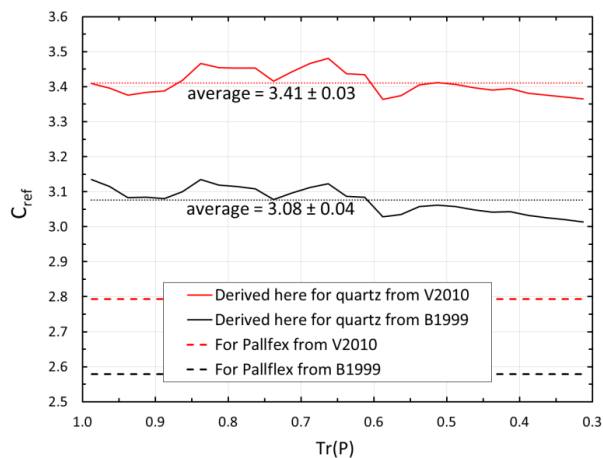


565

566 Figure 4. Average $\sigma_{\text{ap}}(\text{quartz})/\sigma_{\text{ap}}(\text{Pallflex})$ in 0.025 bins of transmittance of Pallflex filter at $\lambda = 530$
 567 nm. Both $\sigma_{\text{ap}}(\text{quartz})$ and $\sigma_{\text{ap}}(\text{Pallflex})$ were corrected both either according to Bond et al. (1999) with

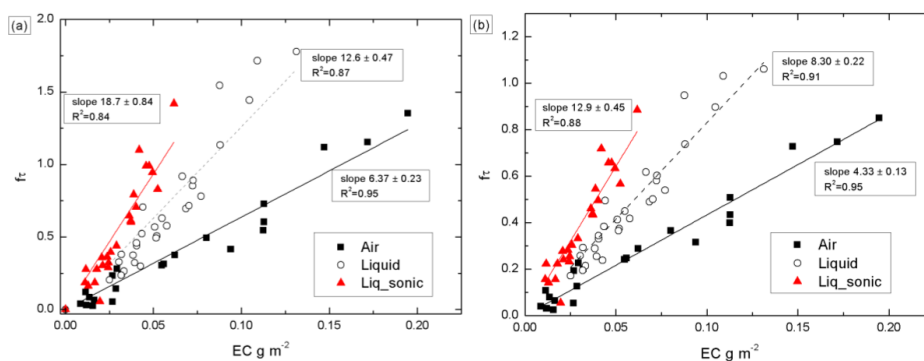


568 the Ogren (2010) modification (O2010) and Virkkula (2010) (V2010) using four values for the single-
 569 scattering albedo ω_0 .



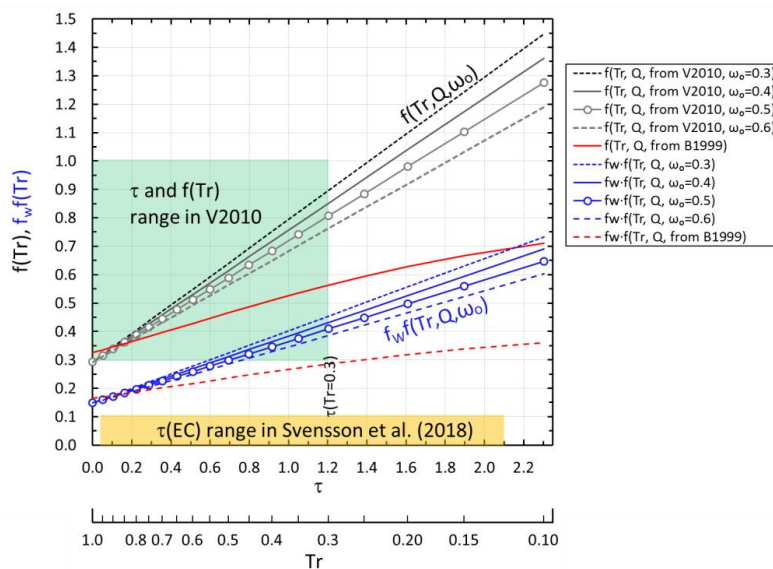
570
 571 Figure 5. The multiple-scattering correction factor C_{ref} for quartz and Pallflex filters in 0.025 bins of
 572 transmittance of Pallflex filter at $\lambda = 530$ nm. The straight lines for C_{ref} of O2010 and V2010 are those
 573 shown in Eqs. (9) and (12).

574



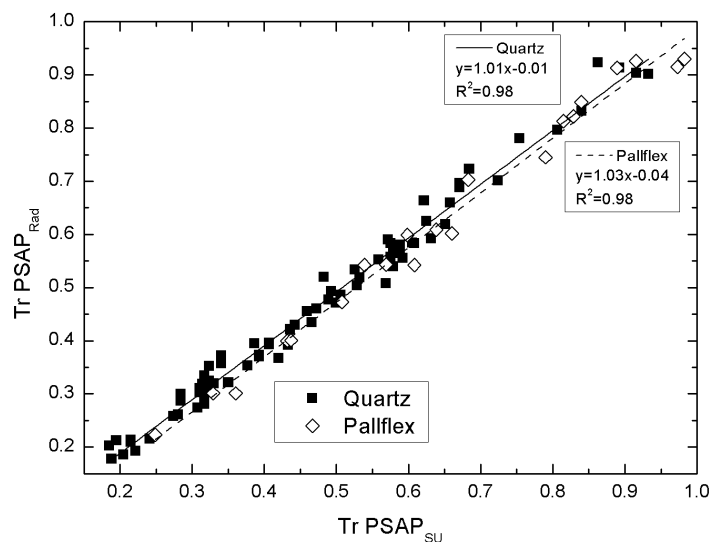
575
 576
 577 Figure 6. Linear regressions of transmittance-corrected optical depth $f_{\tau}(\lambda = 530$ nm) vs. EC of the BC
 578 particles blown into the mixing chamber (Air), into water (Liquid) and blown into water and treated in
 579 the ultrasonic bath (Liq_sonic). The optical depths were corrected with a) the $f_{\tau}(Tr, V2010, \omega_0=0.4)$ and
 580 b) $f_{\tau}(Tr, Q, O2010)$. The regressions were calculated by forcing offset to 0.

581



582

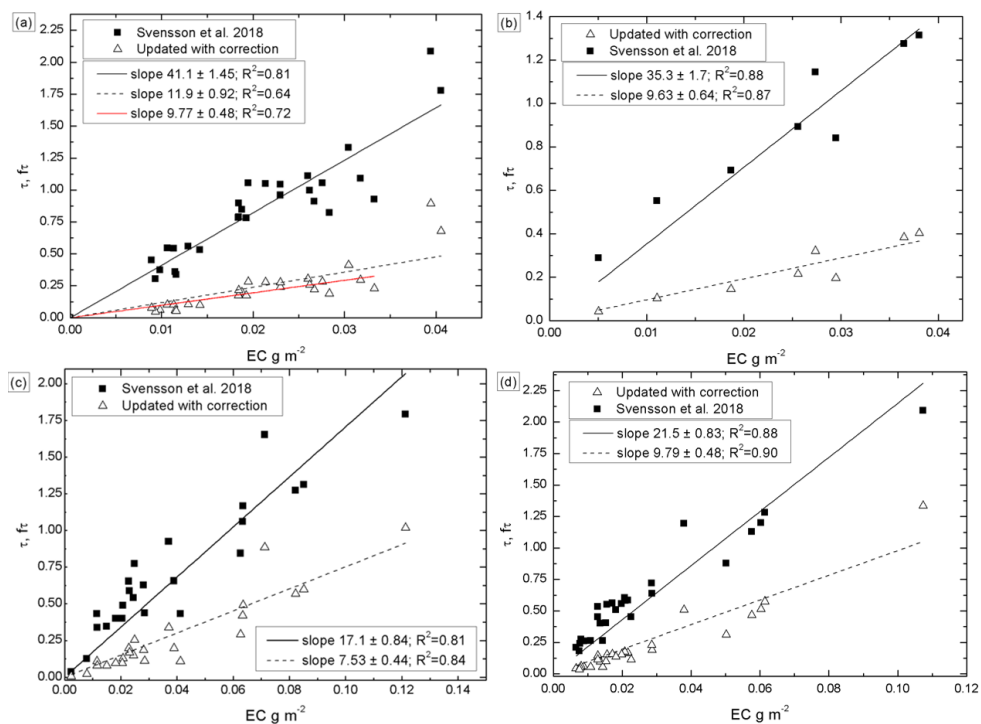
583 Figure 7. Loading correction functions derived from V2010 and O2010 for airborne BC particles
 584 collected on quartz filters (grey lines, $f(\text{Tr}, Q, \omega_o)$) and for BC particles mixed in water and filtered
 585 through similar quartz filters (blue lines, $f_w f(\text{Tr}, Q, \omega_o)$). The green shadowed area shows the range of
 586 optical depths and $f(\text{Tr})$ of the V2010 Pallflex filter calibration and the yellow shadowed line shows the
 587 range of optical depths of EC in snow presented by Svensson et al. (2018).



588

589 Figure 8. Transmittance for quartz and Pallflex filters measured with PSAP radiance research and the
 590 Stockholm University custom-built PSAP.

591



592

593

594 Figure 9. Reanalysis of linear regressions presented by Svensson et al. (2018). a) chimney soot, with
 595 the red line showing the slope with the two points with the highest EC content are excluded, b) NIST
 596 soot, c) field samples from the Indian Himalaya, d) field samples from Finnish Lapland. On the x axis
 597 there is the EC concentration as g m⁻² and on the y axis the non-corrected and corrected optical depth,
 598 τ and ft, respectively.